CONTACTLESS INDUCTIVE FLOW TOMOGRAPHY: THEORY AND EXPERIMENT

Frank Stefani, Thomas Gundrum, and Gunter Gerbeth

1. Introduction

The determination of flow velocities in opaque fluids is a notorious problem in various industrial applications, including steel casting and silicon crystal growth. Obviously, the usual optical flow measurement techniques, as Laser Doppler Anemometry (LDA) or Particle Image Velocimetry (PIV), are not applicable in those cases. Actually, there are a few measurement techniques for opaque fluids, including Ultrasonic Doppler Velocimetry (UDV), mechano-optical probes, and electric potential probes [1]. However, for hot and/or chemically aggressive materials it would be most desirable to avoid any contact with the melt. The wish to reconstruct the sodium velocity in the Riga dynamo experiment [2] by an appropriate contactless method was another strong motivation for the present work.

With view on these possible applications, this report describes a *Contactless Inductive Flow Tomography* (CIFT) for electrically conducting melts, based on external magnetic field measurements. In contrast to traditional inductive flow determination based on electric potential measurements [3], the new method is restricted to fluid flows with not too small magnetic Reynolds numbers. Another shortcoming may be the fact that the method is not very accurate in the determination of local velocities. However, this point might be outweighed by the fact that the method enables online monitoring of transient flow fields in the entire fluid volume, at least with a time-resolution of a few seconds. This feature makes the method attractive for a number of technological and research applications.

2. Basic theory

When an electrically conducting medium, moving with the velocity $\mathbf{u}$, comes under the influence of an imposed steady magnetic field $\mathbf{B}_0$, an electromotive force (emf) $\mathbf{u}\times\mathbf{B}_0$ is induced that drives an electric current

$$\mathbf{j}_0 = \sigma(\mathbf{E}_0 + \mathbf{u}\times\mathbf{B}_0)\,, \tag{1}$$

where σ is the electrical conductivity of the fluid, and $\mathbf{E}_0$ is the electric field which results from the emf. The current $\mathbf{j}_0$, in turn, produces an additional magnetic field $\mathbf{b}$, so that the total current $\mathbf{j}$ becomes also dependent on the total magnetic field $\mathbf{B} = \mathbf{B}_0 + \mathbf{b}$,

$$\mathbf{j} = \sigma(\mathbf{E} + \mathbf{u}\times\mathbf{B})\,. \tag{2}$$

The ratio of the induced magnetic field $\mathbf{b}$ to the imposed magnetic field $\mathbf{B}_0$ is governed by the so-called magnetic Reynolds number

$$Rm = \mu\sigma LU\ , \tag{3}$$

where μ is the magnetic permeability of the fluid, and L and U are typical length and

velocity scales of the flow, respectively. This dimensionless number is, in the most relevant technical applications, smaller than one.

We start from Eq. (2) and employ Biot-Savart's law for the magnetic field and Green's theorem for the electric potential [4,5]. In the following, we will only need the version for the steady case, in which the electric field can be expressed by the gradient of the electric potential, $\mathbf{E} = -\nabla\phi$. The generalization to the time-dependent case can be found in [6]. The integral equation system consists of one equation for the induced magnetic field in the entire volume D of the fluid,

$$\mathbf{b}(\mathbf{r}) = \frac{\sigma\mu_0}{4\pi}\int_D \frac{\big(\mathbf{u}(\mathbf{r}')\times\mathbf{B}(\mathbf{r}')\big)\times(\mathbf{r}-\mathbf{r}')}{|\mathbf{r}-\mathbf{r}'|^3}\,dV' - \frac{\sigma\mu_0}{4\pi}\oiint_S \phi(\mathbf{s}')\,d\mathbf{S}'\times\frac{\mathbf{r}-\mathbf{s}'}{|\mathbf{r}-\mathbf{s}'|^3}\quad , \tag{4}$$

and one equation for the electric potential at the fluid boundary S,

$$\phi(\mathbf{s}) = \frac{1}{2\pi}\int_D \frac{\big(\mathbf{u}(\mathbf{r}')\times\mathbf{B}(\mathbf{r}')\big)\cdot(\mathbf{s}-\mathbf{r}')}{|\mathbf{s}-\mathbf{r}'|^3}\,dV' - \frac{1}{2\pi}\oiint_S \phi(\mathbf{s}')\,d\mathbf{S}'\cdot\frac{\mathbf{s}-\mathbf{s}'}{|\mathbf{s}-\mathbf{s}'|^3}\quad . \tag{5}$$

In Eq. (4) we see that the induced magnetic field $\mathbf{b}$ depends on both the induced primary currents in the volume D and the induced electric potential ϕ at the fluid boundary S. Eqs. (4) and (5) are valid for arbitrary values of Rm, and provide a suitable mathematical set-up to handle dynamos in arbitrary domains [5]. For small Rm, however, the induced magnetic field $\mathbf{b}$ under the volume integrals on the r.h.s. of Eqs. (4) and (5) can be neglected and the total $\mathbf{B}$ can be replaced by $\mathbf{B}_0$.

In [4] we had shown that the velocity structure of the flow can be reconstructed from the external measurement of an appropriate component of the induced magnetic field (e.g., the radial component for a spherically shaped fluid volume) and the induced electric potential at the fluid boundary. There remains a non-uniqueness concerning the radial distribution of the flow [7] what can be made plausible by representing the fluid velocity by two scalars living in the whole fluid volume (e.g., the toroidal and poloidal parts). Then it is clear that two quantities measured on a two-dimensional covering of the fluid give not enough information for the reconstruction of the two desired 3D-quantities.

In [8] we had developed a general method to avoid the electric potential measurement at the fluid boundary. The main idea is to apply the external magnetic field in two different, e.g. orthogonal, directions and to measure both corresponding sets of induced magnetic fields. The main obstacle for the application of this method comes from the electric potential term at the boundary, the measurement of which we just like to circumvent. For the very special case of a spherical fluid volume, it can easily be seen, from multiplying Eq. (4) with the radial unit vector, that the radial component of $\mathbf{b}$ is unaffected by ϕ. For other than spherical fluids, however, there is always an influence of the surface term on $\mathbf{b}$. How can the influence of ϕ be taken into account without measuring it?

In the following we sketch the solution of this puzzle. Assume, for a given $\mathbf{B}_0$, all measured induced magnetic field components be collected into an NB-dimensional vector with the entries $b_i^{(B_0)}$. Assume further a certain discretization of the electric potential at the surface,

denoted by an NP-dimensional vector with the entries $\phi_m^{(B_0)}$. The velocity in the domain D is discretized as an NV-dimensional vector with the entries u_k. Then, Eqs. (4) and (5) can be written in the form

$$b_i^{(B_0)} = K_{ik}^{(B_0)} u_k + L_{im} \phi_m^{(B_0)} \qquad (6) \qquad \text{and} \qquad \phi_m^{(B_0)} = M_{mk}^{(B_0)} u_k + N_{mn} \phi_n^{(B_0)} \qquad (7)$$

with $\mathbf{K}^{(B_0)}$ being a matrix of type (NB, NV), $\mathbf{L}$ a matrix of type (NB, NP), $\mathbf{M}^{(B_0)}$ a matrix of type (NP, NV), and $\mathbf{N}$ a matrix of type (NP, NP). Note that only the matrices $\mathbf{K}^{(B_0)}$ and $\mathbf{M}^{(B_0)}$ depend on the applied magnetic field $\mathbf{B}_0$, whereas the matrices $\mathbf{L}$ and $\mathbf{N}$ are independent of $\mathbf{B}_0$.

As it is well known from magnetoencephalography [9], the inversion of Eq. (7) is a bit tricky due to the singularity of the matrix $(\mathbf{I} - \mathbf{N})$. However, by applying the so-called deflation method [9], one ends up with a single linear relation between the desired velocity field and the measured magnetic field in the form

$$b_i^{(B_0)} = K_{ik}^{(B_0)} u_k + L_{im} (I - N)_{mn}^{-1,defl} M_{nk}^{(B_0)} u_k \quad , \qquad (8)$$

where we have used the superscript '*defl*' in order to indicate the deflation method for the inversion of the matrix $(\mathbf{I} - \mathbf{N})$.

Despite the far-reaching similarity, there is one essential difference of our method compared to magnetoencephalography. While in the latter method one has to determine a single neuronal current distribution, in our case we can produce *quite different current distributions from the same flow field* just by applying various external magnetic fields $\mathbf{B}_0$ subsequently. For each applied magnetic field $\mathbf{B}_0$ we can measure the corresponding induced fields $b_i^{(B_0)}$, and utilize all of them together for the reconstruction of the flow.

For the data analysis of the experiment we will circumvent the remaining non-uniqueness problem by the use of Tikhonov regularization and the method of Tikhonov's L-curve [9]. Note that the inversion of Eq. (8) is equivalent to the minimization of the mean quadratic deviation of the measured fields $b_{i,meas}^{(B_0)}$ from the fields $b_i^{(B_0)}[\mathbf{u}]$ that are modeled according to Eq. (8). Within the regularization one adds to the functional of mean quadratic residual one or more „penalty" functions which are chosen, for convenience, as quadratic functionals of the velocity. For our purpose we minimize the total cost functional

$$F[\mathbf{u}] = F_{B_{0x}}[\mathbf{u}] + F_{B_{0z}}[\mathbf{u}] + F_{div}[\mathbf{u}] + F_{reg}[\mathbf{u}] \qquad (9)$$

with the individual parts

$$F_{B_{0x}}[\mathbf{u}] = \sum_{i=1}^{NB} \frac{1}{\sigma_{i,B_{0x}}^2} \left(b_{i,meas}^{(B_{0x})} - b_i^{(B_{0x})}[\mathbf{u}] \right)^2 \quad , \qquad (10)$$

$$F_{B_{0z}}[\mathbf{u}] = \sum_{i=1}^{NB} \frac{1}{\sigma_{i,B_{0z}}^2} \left(b_{i,meas}^{(B_{0z})} - b_i^{(B_{0z})}[\mathbf{u}] \right)^2 \quad , \qquad (11)$$

$$F_{div}[\mathbf{u}] = \frac{1}{\sigma_{div}^2} \sum_{k=1}^{NV} (\nabla \cdot \mathbf{u})_k^2 \Delta V_k \quad , \tag{12}$$

$$F_{reg}[\mathbf{u}] = \frac{1}{\sigma_{pen}^2} \sum_{k=1}^{NV} \mathbf{u}_k^2 \Delta V_k \quad . \tag{13}$$

The first two functionals represent, for applied transverse field $\mathbf{B}_{0x}$ and axial field $\mathbf{B}_{0z}$, respectively, the mean squared residual deviation of the measured induced magnetic fields $b_{i,meas}^{(B_0)}$ from the fields $b_i^{(B_0)}[\mathbf{u}]$ modeled according to equation (8). $F_{div}[\mathbf{u}]$ enforces the velocity field to be solenoidal, and $F_{reg}[\mathbf{u}]$ is the regularization functional which tries to minimize the kinetic energy. The parameters σ_{i,B_0} are assumed a-priori errors for the measurements of the induced fields. The parameter σ_{div} is chosen very small as it is a measure for the divergence the velocity is allowed to have. The parameter σ_{pen} determines the trade-off between minimizing the mean squared residual deviation of the observed fields and minimizing the kinetic energy of the estimated velocity field. The normal equations that follow from the minimization of the functional (9) are solved by Cholesky decomposition. By scaling the penalty parameter σ_{pen} one can derive the so-called Tikhonov's L curve, i.e., the mean squared residual in dependence on the penalty function. At the point of highest bending (the „knee") we get a good compromise between the fit of the modeled magnetic fields to the measured ones on one hand, and minimum kinetic energy on the other hand [10].

2. Experimental results

In order to demonstrate the feasibility of the contactless inductive velocity reconstruction method in real applications an experiment has been set up in which the propeller driven flow of a liquid metal has to be reconstructed solely from externally measured magnetic field data.

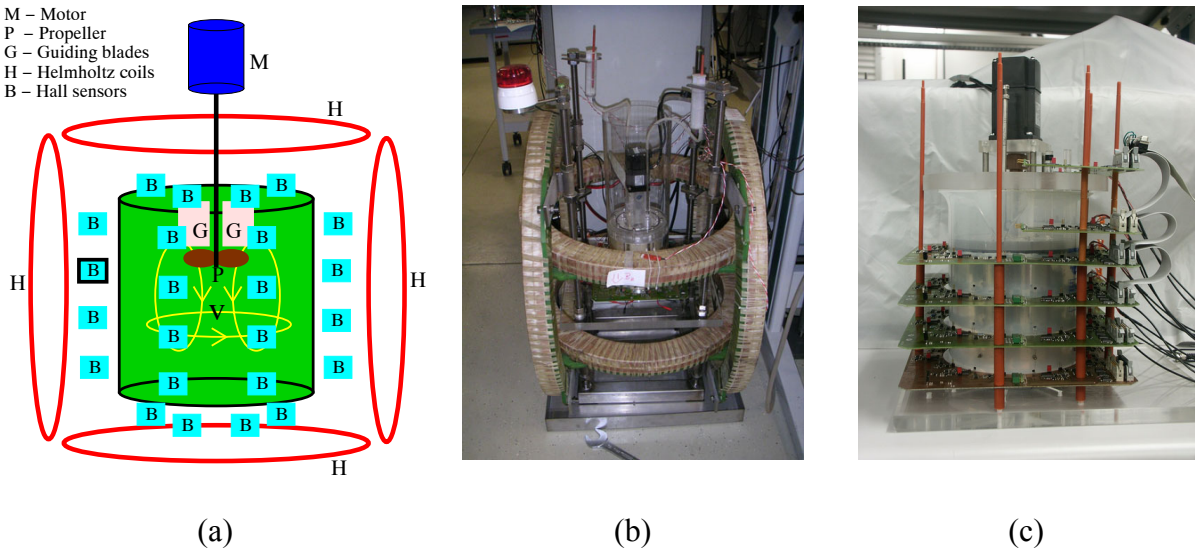

(a) (b) (c)

Fig. 1: The CIFT experiment. Schematic view (a), total view (b), and details of the vessel with the circuit boards for the Hall sensors and AD transformer.

Figure 1 shows the experimental set-up. We use 4.4 liters of the eutectic alloy $Ga^{67}In^{20.5}Sn^{12.5}$ which is liquid at room temperatures. Its density and electrical conductivity at 20°C are 6.36×10^3 kg/m^3 and 3.31×10^6 S/m, respectively. The flow is produced by a motor driven propeller with a diameter of 6 cm inside a polypropylene vessel with 18.0 cm diameter. The height of the liquid metal is 17.2 cm, giving an aspect ratio close to 1.

The propeller can rotate in both directions, resulting either in upward or downward pumping. The rotation rate can reach 2000 rpm producing a mean velocity of 1 m/s, which corresponds to an $Rm \approx 0.4$. The flow structure for the two directions is not symmetric for three reasons. At first, the propeller itself has a preferred direction. At second, it is positioned approximately at one third of the liquid height, measured from the top. At third, there are 8 guiding blades above the propeller, having two functions. For the downward pumping, they are intended to remove the upstream swirl in order not to deteriorate the pressure conditions for the propeller. For the upward pumping they remove the downstream swirl thus leaving the entire flow rather swirl-free. Hence, the downward pumping produces, in addition to the main poloidal roll, a considerable toroidal motion, too. For the upward pumping, this toroidal motion is, to a large extend, inhibited by the guiding blades. It was one of the tasks of the experiment to discriminate between those different flow structures.

Two pairs of Helmholtz coils are fed by currents of 22.5 Ampere and 32.5 Ampere, respectively, to produce altermately an axial and an tranverse field of 4 mT, which both are rather homogeneous throughout the vessel. Either field is applied for a period of 3 seconds, during which a trapezoidal signal form is used. The measurements are carried out for 0.5 seconds, 1 second after the plateau value of the trapezoidal current has been reached. Hence, we get an online monotoring with a time resolution of 6 seconds. The induced magnetic fields are measured with 49 Hall sensors, 8 of them grouped together on each of the 6 circuit boards which are located on different heights (Figs. 1a, 1c). One additional sensor is located in the center below the vessel.

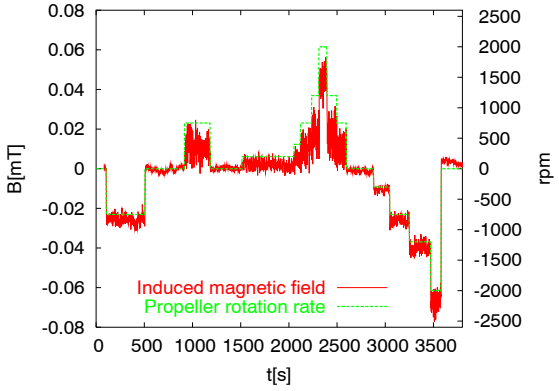

Fig. 2: Propeller rotation rate and Hall sensor signal during one run with applied axial field, as measured by the Hall sensor that is emphazised in Fig. 1a.

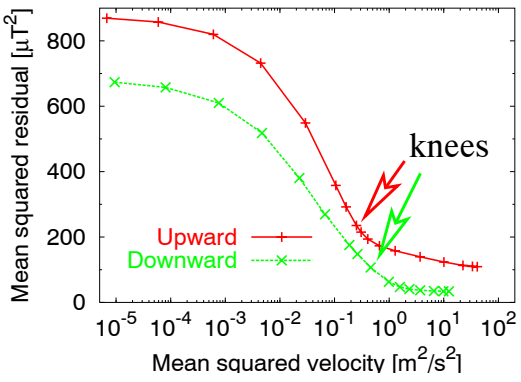

Fig. 3: Tikhonov's L curve, showing the rms in dependence of the mean energy. At the indicated "knees" one obtains a reasonable compromise between data fitting and minimum kinetic energy.

The basic problem for any practical application of the method is the reliable determination of small induced magnetic fields on the background of much larger imposed magnetic fields. For this it is indispensable to have an accurate control of the external magnetic field. In our configuration the current drift in the Helmholtz coils can be controlled with an accuracy of

better than 0.1 per cent. This is sufficient since the measured induced fields are approximately 1 per cent of the applied field.

Another serious problem is the unavoidable temperature drift of the Hall sensors. This concerns their sensitivity as well as the offset. The sensitivity drift is connected with the temperature dependence of the semiconductors resistance and can be overcome by keeping the current constant. The offset problem is overcome by changing the sign of the applied magnetic field. For that purpose, we choose a trapezoidal signal form which changes its sign every 3 seconds. Figure 2 shows that by these means a stable measurement of the small induced field can be realized even over a period of one hour. After the measurement has been accomplished for the applied transversal field $\mathbf{B}_{0x}$, the same procedure is carried out for the applied axial field $\mathbf{B}_{0z}$. For both flow directions, Fig. 3 shows Tikhonov's L-curves with a clear „knee" which is interpreted as the point with the physically most reasonable solution.

For upward and downward pumping, Figs. 4 and 5 show the induced magnetic fields measured at the 49 positions, and the inferred velocity field at 52 discretization points. In Fig. 4c we see the upward flow in the center of the cylinder and the downward flow at the rim, but nearly no rotation of the flow. In Fig. 5c we can identify the downward flow in the center and the upward flow at the rim, together with a rotation of the flow. This absence and presence of the swirl is an important feature which can evidently be discriminated by our method. It is worth to note that not only the structure of the flow, but also the range of the velocity scale is correctly reproduced by the inversion.

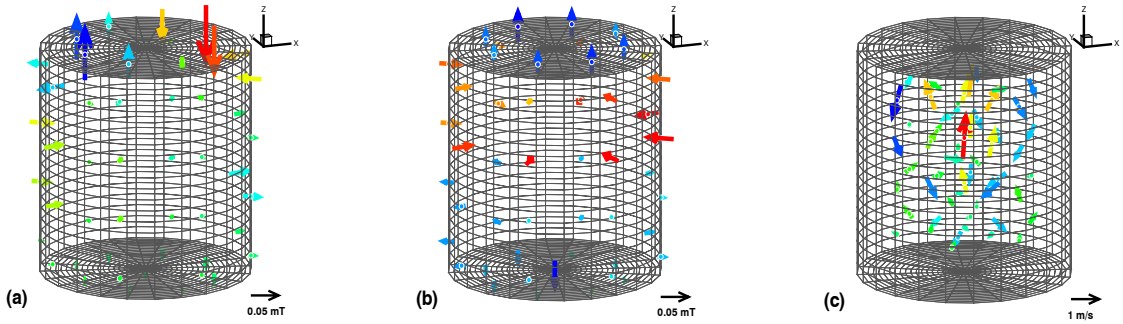

Fig. 4: The measured magnetic fields and the reconstructed velocity field for the case that the propeller pumps upward with 1200 rpm. Measured induced field for transversal applied field (a); measured induced field for applied axial field (b); and reconstructed velocity (c). For (a) and (b) the color coding discriminates between ingoing and outgoing magnetic field lines. For (c) the color coding mirrors the axial component of the velocity.

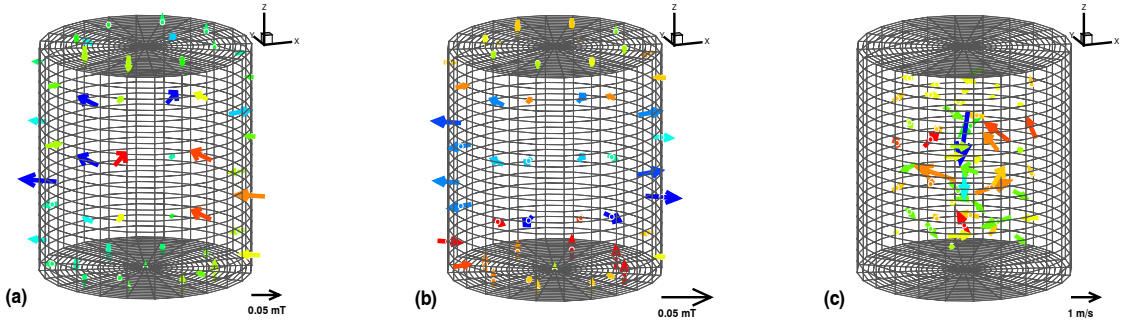

Fig. 5: The same as Figure 4, but for the propeller pumping downward with 1200 rpm.

4. Conclusions and prospects

Flow measurement based on induced electric potentials has a long tradition and a lot of practical applications [3]. The change from induced electric potentials to induced magnetic fields allows a completely contactless measuring technique for those flows whose magnetic Reynolds number is not too small. In a liquid metal experiment, we have put into practice a first version of contactless inductive flow tomography (CIFT), using two orthogonal imposed magnetic fields. A particular power of CIFT consists in a transient resolution of the full three-dimensional flow structure in steps of a few seconds. Due to its weakness, the externally applied magnetic field does not influence the flow to be measured. However, CIFT is also possible in cases where stronger magnetic fields are already present for the purpose of flow control, as, e.g., the electromagnetic brake in steel casting or the DC-field components in silicon crystal growth. The challenges for the future lay with improving the depth resolution of the method by using magnetic fields with variable frequency on one hand, and with the extension of the method to inverse dynamo problems with larger magnetic Reynolds numbers, on the other hand.

Acknowledgement

This work was supported by Deutsche Forschungsgemeinschaft under grant GE 682/10-1/2.We thank Heiko Kunadt for manufacturing the mechanical part of the experiment, and Bernd Caspar for designing the circuit boards.

References

[1] S. Eckert, G. Gerbeth, F. Stefani, and W. Witke (2003), Measuring techniques for liquid metal velocity measurements, in P.D. Lee, A. Mitchell, J.-P. Bellot, A. Jardy (Eds.), Proceedings of the 2003 International Symposium on Liquid Metal Processing and Casting (LMPC 2003) (pp. 261-271), Nancy

[2] A. Gailitis, O. Lielausis, E. Platacis, G. Gerbeth, and F. Stefani (2002), Laboratory experiments on hydromagnetic dynamos, Rev. Mod. Phys., 74, 973

[3] J. A. Shercliff (1962), The theory of electromagnetic flow-measurement, Cambridge, Cambridge University Press

[4] F. Stefani and G. Gerbeth (1999), Velocity reconstruction in conducting fluids from magnetic fields and electric potential measurements, Inverse Problems, 15, 771

[5] M. Xu, F. Stefani, and G. Gerbeth (2004), The integral equation method for a steady kinematic dynamo problem, J. Comp. Phys., 196, 102

[6] M. Xu, F. Stefani, and G. Gerbeth (2003), An integral equation approach to time-dependent kinematic dynamos in finite domains, Phys. Rev E, in press

[7] F. Stefani, G. Gerbeth (2000), On the uniqueness of velocity reconstruction in conducting fluids from measurements of induced electromagnetic fields, Inverse Problems, 16, 1

[8] F. Stefani, G. Gerbeth, A contactless method for velocity reconstruction in electrically conducting fluids (2000), Meas. Sci. Technol., 11, 758

[9] M. Hämäläinen, R. Hari, R. J. Knuutila, and O. V. Lounasmaa (1993), Rev. Mod. Phys., 65, 413

[10] P. C. Hansen (1992), Analysis of discrete ill-posed problems by means of the L-curve, SIAM Review, 34, 561